Operational GMS-5 VISSR Calibration

M. Tokuno*, S. Kurihara* and Y. Kaido*

Abstract

We rewrote the paper "The Status of Calibration of VISSR on board GMS-5" (Kurihara and Tokuno, 2000) in English for users of GMS data in foreign countries. In addition, we reported on the development of a new method without calibration shutter information against the mal-functioning of the calibration shutter system, which occurred irregularly, corresponding to the utilization of GMS-5 over its lifetime.

This paper describes the status of the calibration of VISSR on board GMS-5 and matters requiring attention when using the calibration data on the following subjects:

- Techniques for calibrating visible and infrared channel data
- Correction of previously observed calibration tables of infrared channel data
- Care required and problems encountered on applying infrared channel calibration tables (including observations for satellite wind estimation) and S-VISSR fixed calibration tables operationally
- Doubt regarding the response function of the water vapor channel
- Long term trends of visible channel data

Finally, this paper shows that the new method without calibration shutter information is complete and provides nearly same accurate calibration data as with calibration shutter information.

1. Introduction

The Geostationary Meteorological Satellite 'HIMAWARI 5' (GMS-5) was launched in March 18, 1995 and its data has been utilized in various areas since June 1, 1995. The Visible and Infrared Spin Scan Radiometer (VISSR) on board GMS-5 is an improvement in comparison with that of GMS to GMS-4 as shown in Table 1. The main improvements are as follows: adding the infrared split window channel (infrared 1 and 2) and the water vapor absorption channel. The additional channels provide utilization advantages as follows: an improvement in the accuracy of sea surface temperature by the split window method (McMillin et al., 1984), the detection of ash clouds by temperature difference between split window channels (Potts, 1993, Tokuno, 1997), estimation of the amount of water vapor in the atmosphere and water vapor motion winds (Meteorological Satellite Technical Note Special Volume, 1996).

Also an improvement in the accuracy of solar irradiance is expected as the material of the detector of the visible channel is changed from a Photo Multiplier Tube (PMT) to a Silicon Photo Diode with

*Meteorological Satellite Center, System Engineering Division
(Received August 9, 2000 : Revised November 15, 2000)

more stable sensitivity (Tsuchiya, 1982).

Thus, it is dispensable to correct data obtained from the detector (hereafter referred to as calibration procedure) for maintaining the accuracy of products.

We report on the operational calibration procedure of GMS-5 in Meteorological Satellite Center (MSC) and matters requiring attention when using the calibration data. Lastly, we report on the development of the calibration method for emergency cases when calibration shutter data is not available.

Table1 The characteristic of detectors of GMS 1-4 and GMS-5

	Channel	Bandwidth (μm)	Resolution (km)*1	Detector
GMS1-4	Visible	0.5-0.7	1.25	PMT
	Infrared	10.5-12.5	5	HgCdTe
GMS5	Visible	0.5-0.7	1.25	Silicon-Photo-Diode
	IR-1(Window)	10.5-11.5	5	HgCdTe
	IR-2(Window)	11.5-12.5	5	HgCdTe
	IR-3(H2O)	6.5-7.3	5	HgCdTe

*1:The bandwidth of GMS-5 VISSR is the nominal values.

Infrared channels 1 and 2 are called infrared split channels since the wavelength of the two channels divides the window region of the atmosphere into two regions, while infrared channel 3 is called the water vapor channel since its wavelength is allocated in the water vapor absorption region of the atmosphere.

2. VISSR Calibration

The VISSR on board the spin satellite GMS-5 observes the earth from northwards to southwards along with the rotation of the satellite. Incoming energy is converted to digital data in the VISSR Digital data Modulator (VDM) and is transported to the Command and Data Acquisition Station (CDAS) on the ground. CDAS adds the calibration and navigation information to the data and changes the level of data. These data are called Stretched-VISSR (S-VISSR) and they are transported to the Medium Data User System (MDUS) via GMS-5. The data received in CDAS is transported to the Data Processing Center (DPC) via CDAS. This data is utilized in making calibration and navigation information, WE-FAX and other products.

The production of calibration information is defined as the table in which the count value observed in the satellite is related to a physical energy value such as temperature. To make the table, the equation by which the count value is corresponded to a physical value is obtained, then the calibration table is produced based on the physical value calculated from the count value from the equation.

The VISSR calibration procedure in DPC and CDAS is shown in the following sections.

2.1 Visible Channel Calibration

The visible channel on board GMS-5 observes the earth with the IFOV South-North 35 μ rad, East-West 35 μ rad, and a horizontal resolution of 1.25 km in nadir. The data observed by the detector is converted to six-bit digital data in the satellite. The six-bit digital data is transported to the ground station. The equation for calibration is needed for every detector since the visible channel is composed of four detectors. The concept of visible channel calibration is shown as follows:

First, incoming solar energy (reflectance) is converted to voltage in the detectors of VISSR. The relation between reflectance and voltage is shown in the equation (1) since reflectance has a linear relationship with voltage.

$$V = a A + V_0 \quad (1)$$

where A is reflectance, V_0 is voltage when the sensor observes space with reflectance at zero, a is coefficient.

Next, voltage is converted into count value in VDM in Eq. (2).

$$C = b_0 + b_1\sqrt{V} \quad (2)$$

where V is voltage, C is count value, b_0, b_1 are coefficients.

The coefficients are constant values determined by ground experiments before launch.

Using equations (1) and (2), the relation between reflectance and count value is shown in Eq. (3).

$$A = (C - b_0)^2 / b_1^2 a - V_0 / a \quad (3)$$

The satellite has a function called the "solar correction function" to measure solar radiance reduced by 50% through the purism on board the satellite. It is possible to determine coefficient "a" in equation (3) owing to the function together with V_0 measured from the radiance of space. This procedure is usually called the calibration procedure for the visible channel. However, it is difficult to measure solar radiance with high accuracy at present. Therefore, the constant values measured by ground experience before launch are used as the coefficients "a" and 'V_0."

The calibration table related to radiance and count value is constant as the coefficients in equation (3) are constant. The constant visible calibration tables are respectively used for every visible detector since the visible channel is composed of four detectors. Therefore, if four detectors have different individual sensitivities an image produced from a raw count value has an irregular characteristic caused by the difference in sensitivity between the detectors.

To minimize the cause of this, a special procedure called "normalization" is performed in DPC. In this procedure, the calibration tables for the three other detectors are converted based on the calibration table of the detector determined to be standard among the four detectors. Detector number two was selected as the standard detector because its sensitivity is more stable than the other three detectors based on the results of an investigation before the operation. This investigation was performed once, soon after operation, as the difference in sensitivity between the visible detectors has been little changed up to now in the operation of DPC.

S-VISSR data has the additional standard calibration table as explained later to help users of the fixed conversion table. Four original calibration tables are converted to the standard calibration table. In this procedure, the count value observed by the detectors is converted to reflectance by referring to the calibration tables in DPC, then the converted reflectance is converted to the count value by referring to the standard calibration table. Visible data of S-VISSR disseminated to MDUS are produced through the series of procedures mentioned above.

2.2 Infrared Channel Calibration

Infrared channels on board GMS-5 are composed of three channels, i.e., infrared channel 1 (IR1, 10.5 - 11.5 μm), infrared channel 2 (IR2, 11.5 - 12.5 μm), infrared channel 3 [IR3 (WV), 6.5 - 7.3 μm]. Each channel has an IFOV with 140 μrad for north-south directions and 140 μrad for east-west directions (approximately 5 km horizontal resolution in nadir). Observed data is sent to the ground station after it is converted to 8 bits digital data in the satellite. The infrared channels' calibration procedure is shown below.

Incoming energy (radiance) is converted to voltage in the detector of VISSR. The relationship between voltage and radiance is shown in Eq. (4) as incoming radiance has a linear relation to voltage.

$$V = d E + V_0 \quad (4)$$

where E is radiance observed by the detector, V_0 is the voltage when VISSR observes space and d is the coefficient.

Then voltage is converted to a digital count in VDM as shown in Eq. (5)

$$C = C_0 + C_1 V \quad (5)$$

where C_0 and C_1 are coefficients determined from the result of the test on the ground.

The relationship between digital count and radiance is shown in Eq. (6) using Eq. (4) and (5).

$$E = (C - C_0) / C_1 d - V_0 / d \quad (6)$$

In addition, the relationship between radiance and temperature is shown in Eq. (7).

$$E(\lambda, T) = \varepsilon \int \Psi(\lambda) B(\lambda, T) d\lambda / \int \Psi(\lambda) d\lambda \quad (7)$$

where ε, $\Psi(\lambda)$ and $B(\lambda, T)$ are emissivity (= 1.0, when VISSR observes the earth), response function and plank function respectively. λ and T are wavelength and temperature.

A conversion table to relate between digital count and temperature is made using Eq. (6) and (7). Coefficients V_0 and d are variable in every observation, though coefficients C_0 and C_1 in Eq. (6) are constant. Therefore, it is necessary to estimate coefficients V_0 and d at every observation in the infrared channel calibration procedure.

We can estimate coefficients V_0 and d in the following procedure:

We can estimate coefficient V_0 in the correction procedure when VISSR observes space. In this procedure, we first get the digital count when VISSR observes space. Assuming the radiance is zero when VISSR observes space, Eq. (8) is made from Eq. (6).

$$V_0 = (Csp - C_0) / C_1 \quad (8)$$

where Csp is the digital count when VISSR observes space.

Next, we can estimate coefficient d in the correction procedure when VISSR observes the standard blackbody in the satellite. In this procedure, we first get the digital count and temperature when VISSR observes the standard blackbody in the satellite. The temperature is the temperature of the standard blackbody which is considered the temperature of the detector and scan mirror et al. (hereafter referred to as the effective shutter temperature, Te). Radiance corresponding to Te is estimated in Eq. (9) added Te in Eq. (7). We can get coefficient d in Eq. (10), which is made from Eq. (6) substituted Te and radiance.

$$E_{bl}(\lambda, Te) = \varepsilon \int \Psi(\lambda) B(\lambda, Te) d\lambda / \int \Psi(\lambda) d\lambda \quad (9)$$

$$d = C_{bl} - C_0 / C_1 E_{bl} - V_0 / E_{bl} \quad (10)$$

where C_{bl} and E_{bl} are the digital count and radiance when VISSR observes the standard blackbody.

The above procedure is carried out for every standard observation (24 times in a day) except for wind observation and limited observation in DPC, and then a calibration table related between the digital count and temperature is produced. However, we used the calibration table produced on the previous day as shown in Figure 1, since the above procedure is not finished before producing an image as S-VISSR data produced in CDAS. In this table, the cold temperature

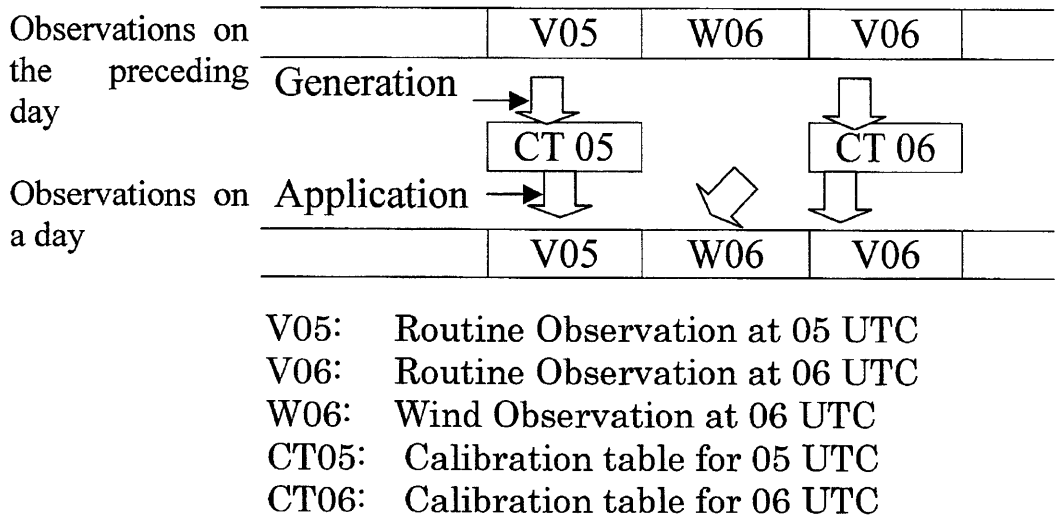

Figure 1 Producing calibration table and the timing to reflect its table.
The previous calibration table for normal conditions (CTO6) is used for wind observation (W06).

region is corresponded to low brightness level and inverse warm temperature region to high brightness level. We use this calibration table in DPC while in the case of S-VISSR an alternative calibration table for S-VISSR is produced after we add the reverse and shift procedure to the calibration table.

Figure 2 shows the concept of reverse procedure. In the reverse procedure, observed brightness level

Observation Level	Revesed Level	Temperature
0	255	T0
1	254	T1
⋮	⋮	⋮
n	255-n	Tn
⋮	⋮	⋮
254	1	T254
255	0	T255

Figure 2 The concept of reverse procedure (infrared channel).
(Tn is temperature at observed level n)
n level is reversed to 255-n level. In this procedure, we produce the conversion table in which the reversed level is converted to temperature.

(hereafter referred to as observed level n) is reversed to (255-n), for example 0 level to 255 level and 1 level to 254 level as shown in Figure 2. Then the table in which the observed level is converted to the reversed level is produced. As a result, the low temperature is corresponded to the high brightness level and the high temperature to the low brightness level.

A concept of shift procedure is shown in Figure 3. The shift procedure is carried out by adjusting the fixed calibration table (hereafter referred to as the fixed table) produced from the results of the ground test to the above calibration table as accurately as possible. In this procedure we get a difference (hereafter referred to as level-difference) between the level in the fixed table and the reversed level at 200 K as shown in procedure-1 of Figure 3. Then we produce the level for S-VISSR (hereafter referred to as S-VISSR level) adjusting the reverse level using level-difference to produce a table in which the reverse level is corresponded to the S-VISSR level as shown in procedure-2 of Figure 3.

We carry out both the reserved procedure and the shift procedure simultaneously when producing the image routinely. We produce the conversion table in

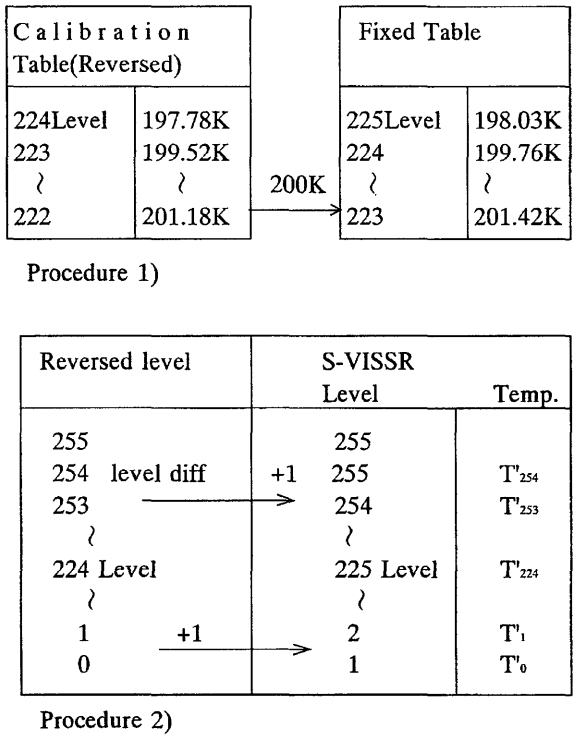

Figure 3 The concept of shift procedure (infrared channel)
(Tn is temperature at reversed level)
procedure 1) we calculated the level difference between the fixed table and the reversed table at a level which corresponds to temperature that is closest to and greater than 200 K. In this case, the 222 level of the reversed calibration table corresponds to the 223 level of the fixed calibration table, and the level difference between the two tables is one level.
procedure 2) we added the level difference to the reversed level, and we produced the table related between the reversed level and the S-VISSR level.

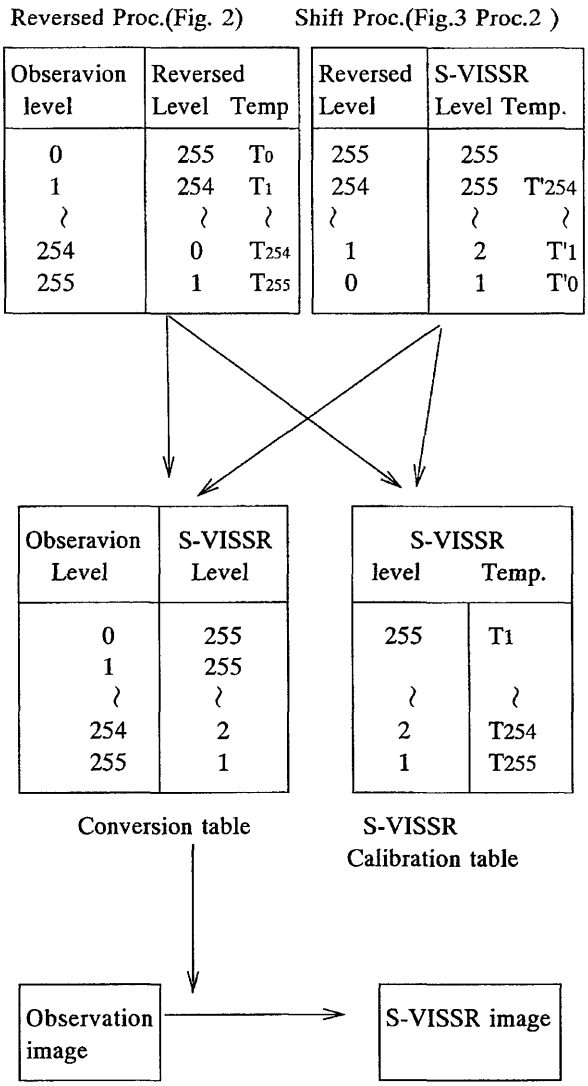

Figure 4 The concept of change of the infrared calibration procedure operationally
The reversed procedure and the shift procedure are performed simultaneously.
We produced 'the conversion table' and 'S-VISSR calibration table' in which the observed level is converted to the S-VISSR level by using the table related between the observed level and the reversed level.

which the observed level is converted to the S-VISSR level using the table in which the observed level is converted to the reversed level, the table in which the reversed level is converted to the S-VISSR level and the table in which the S-VISSR level is converted to temperature. In CDAS, observed image data is converted to S-VISSR image data using the S-VISSR conversion table (Figure 4).

3. Notes on Utilization of Infrared Channel Data

3.1 Modification of Infrared Channel Calibration

As we had used emissivity with error in Eq. (9) from V6 on June 13, 1996, at which GMS-5 operation routinely started to V23 on November 29, 1996, the temperature was estimated lower than that calculated using real emissivity. For example, the temperature of IR1, IR2 and IR3 corresponded to the level at 300K on the calibration table were estimated approximately 1.7K, 1.8K and 1.1K lower than that estimated using real emissivity. To cope with this failure, MSC was carried out reproducing the calibration table during the above term. We also prepared the easy-conversion

Table 2　Simplified correction table

This table shows the correction value for correcting the infrared calibration tables from 06 UTC June 13 1995 to 23 UTC November 29 1996.
Corrected Temperature (K) = Temperature (K) + Correction Value

Temp. (K)	correction(K)			Temp. (K)	correction(K)			Temp. (K)	correction(K)			Temp. (K)	correction(K)			Temp. (K)	correction(K)		
	IR1	IR2	WV		IR1	IR2	WV		IR1	IR2	WV		IR1	IR2	WV		IR1	IR2	WV
200	0.76	0.81	0.49	225	0.97	1.03	0.62	250	1.19	1.18	0.77	275	1.44	1.52	0.93	300	1.70	1.81	1.10
201	0.77	0.82	0.50	226	0.98	1.04	0.63	251	1.20	1.20	0.77	276	1.45	1.54	0.94	301	1.71	1.82	1.11
202	0.78	0.83	0.50	227	0.98	1.05	0.63	252	1.21	1.22	0.78	277	1.46	1.55	0.94	302	1.72	1.83	1.12
203	0.79	0.84	0.51	228	0.99	1.06	0.64	253	1.22	1.24	0.79	278	1.47	1.56	0.95	303	1.73	1.84	1.13
204	0.79	0.85	0.51	229	1.00	1.06	0.64	254	1.23	1.26	0.79	279	1.48	1.57	0.96	304	1.75	1.85	1.13
205	0.80	0.85	0.52	230	1.01	1.07	0.65	255	1.24	1.28	0.80	280	1.49	1.58	0.96	305	1.76	1.86	1.14
206	0.81	0.86	0.52	231	1.02	1.08	0.66	256	1.25	1.30	0.80	281	1.50	1.59	0.97	306	1.77	1.88	1.15
207	0.82	0.87	0.53	232	1.03	1.09	0.66	257	1.26	1.32	0.81	282	1.51	1.60	0.98	307	1.78	1.89	1.16
208	0.83	0.88	0.53	233	1.04	1.10	0.67	258	1.27	1.34	0.82	283	1.52	1.61	0.98	308	1.79	1.90	1.16
209	0.83	0.89	0.54	234	1.04	1.11	0.67	259	1.28	1.36	0.82	284	1.53	1.62	0.99	309	1.80	1.91	1.17
210	0.84	0.90	0.54	235	1.05	1.12	0.68	260	1.29	1.37	0.83	285	1.54	1.63	1.00	310	1.81	1.92	1.18
211	0.85	0.91	0.55	236	1.06	1.13	0.68	261	1.30	1.38	0.84	286	1.55	1.65	1.00	311	1.83	1.94	1.19
212	0.86	0.91	0.55	237	1.07	1.14	0.69	262	1.31	1.39	0.84	287	1.56	1.66	1.01	312	1.84	1.95	1.19
213	0.87	0.92	0.56	238	1.08	1.15	0.70	263	1.32	1.40	0.85	288	1.57	1.67	1.02	313	1.85	1.96	1.20
214	0.88	0.93	0.56	239	1.09	1.16	0.70	264	1.33	1.41	0.86	289	1.58	1.68	1.02	314	1.86	1.97	1.21
215	0.88	0.94	0.57	240	1.10	1.17	0.71	265	1.33	1.42	0.86	290	1.59	1.69	1.03	315	1.87	1.98	1.22
216	0.89	0.95	0.57	241	1.11	1.18	0.71	266	1.34	1.43	0.87	291	1.60	1.70	1.04	316	1.88	2.00	1.22
217	0.90	0.96	0.58	242	1.12	1.19	0.72	267	1.35	1.44	0.88	292	1.61	1.71	1.05	317	1.89	2.01	1.23
218	0.91	0.97	0.58	243	1.13	1.20	0.73	268	1.36	1.45	0.88	293	1.63	1.72	1.05	318	1.91	2.02	1.24
219	0.92	0.97	0.59	244	1.13	1.21	0.73	269	1.37	1.46	0.89	294	1.64	1.74	1.06	319	1.92	2.03	1.25
220	0.92	0.98	0.59	245	1.14	1.22	0.74	270	1.38	1.47	0.89	295	1.65	1.75	1.07	320	1.93	2.04	1.26
221	0.93	0.99	0.60	246	1.15	1.23	0.74	271	1.39	1.48	0.90	296	1.66	1.76	1.08				
222	0.94	1.00	0.61	247	1.16	1.24	0.75	272	1.41	1.49	0.91	297	1.67	1.77	1.08				
223	0.95	1.01	0.61	248	1.17	1.25	0.76	273	1.42	1.50	0.92	298	1.68	1.78	1.09				
224	0.96	1.02	0.62	249	1.18	1.26	0.76	274	1.43	1.51	0.92	299	1.69	1.79	1.10				

table as shown in Table 2 to easily correct the temperature of infrared channel data accumulated by past users. Also, in addition to the easy-conversion table, we prepared the corrected calibration table for each observation. The corrected calibration table is accumulated in every image data preserved in DPC.

3.2 Error Depended on Previous Day's Utilization of Calibration Table

The infrared channels' calibration procedure uses the calibration table from the previous day (hereafter referred to as the previous table) as mentioned in section 2.2. Figure 5 shows the concept of comparing the calibration table, which is made using observed data on the day (hereafter the day table) with the previous table. The figure shows that the temperature difference at the level between the day table and the previous table is apt to increase from the low to the high temperature region. Therefore, we investigated the temperature difference in the low and high temperature regions.

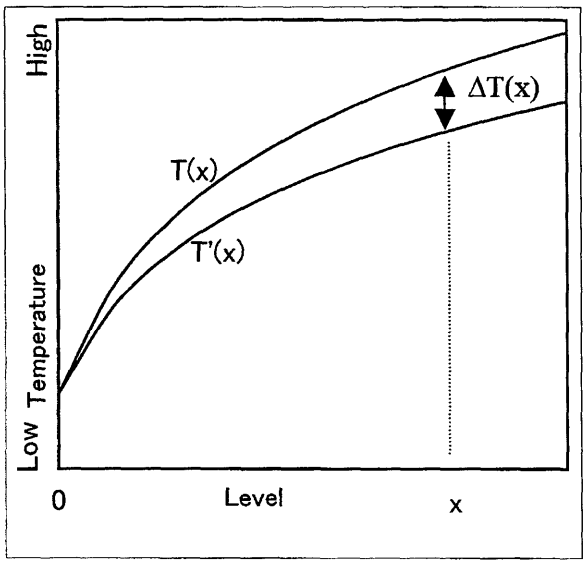

Figure 5　A concept compared the calibration table, which is made using observed data in the day (T(x) with the previous table (T'(x)). Δ x = T(x) - T'(x)

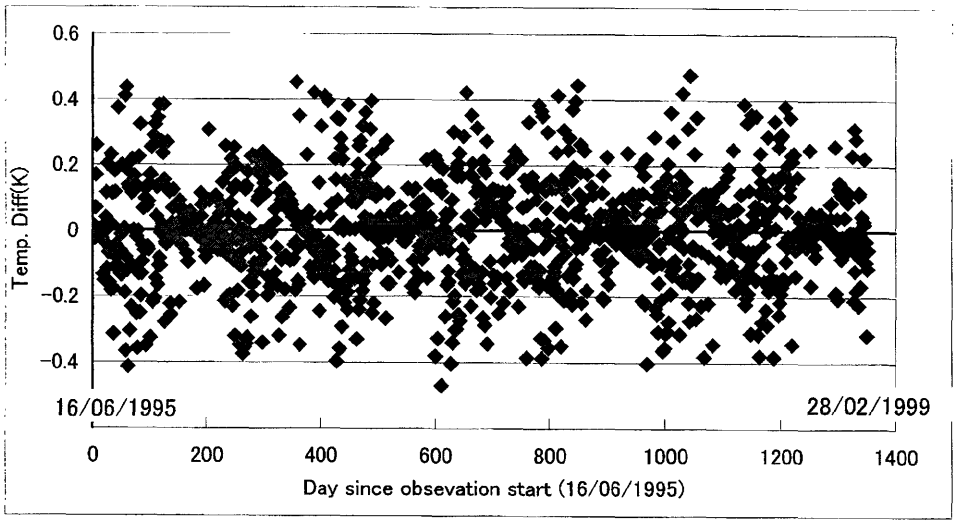

Figure 6 The annual change of temperature difference between using the day table and the previous table for the high temperature region corresponding to the 150 digital count (approximately 290K) of IR1 at no-eclipse observation V0 from 16 June 1995 to 28 February 1999.

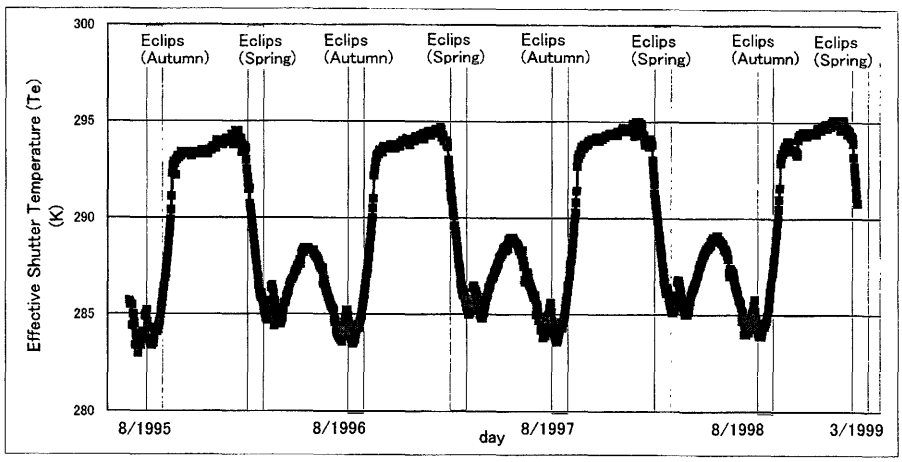

Figure 7 Variability of effective shutter temperature (Te) at V16. The shadow area corresponds to the eclipse period.

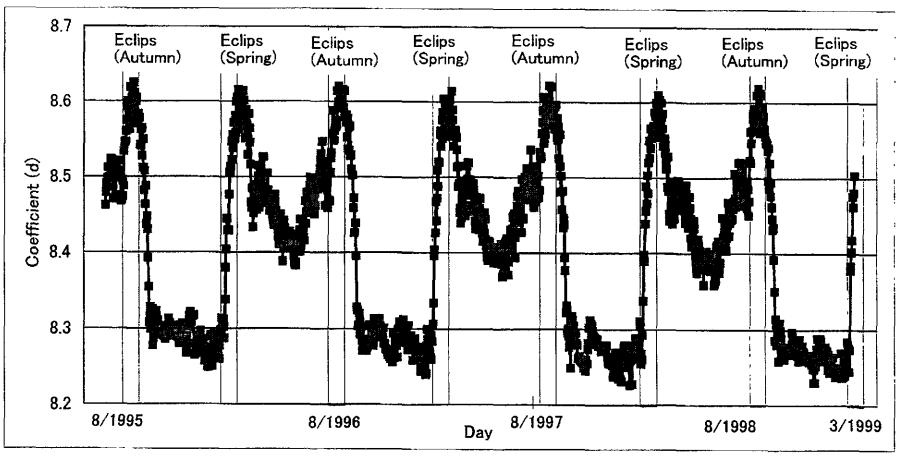

Figure 8 Variability of coefficient d in Eq. (6), which represents the relation between the digital count and radiance at V16. The shadow area corresponds to the eclipse period.

Figure 6 shows the annual change in temperature difference (hereafter referred to as ΔTx for error) between using the day table and the previous table for the high temperature region corresponding to a 150 digital count (approximately 290 K) of IR1 at no-eclipse observation V_0. The results of statistics using all data from June 16, 1995 to February 28, 1999, (the total number of data is 1342), showed that the mean of error is 0.00K, standard deviation is 0.15K and maximum error is 0.48K. The same statistic carried out for the high temperature region corresponding to a 150 digital count of IR2, low temperature region corresponding to a 60 digital count (approximately 235K) of IR1 and IR2, and a 40 digital count (approximately 245K). The result shows that the mean of error, standard deviation and maximum error are respectively 0.00K, 0.16K and 0.56K for the high temperature region of IR2. On the other hand, the mean of error, standard deviation and maximum error are respectively 0.00K, 0.10K for the low temperature region of IR1, IR2 and WV, however, maximum error is largest (0.39K) for IR1 and IR2, followed by WV (0.31K).

Next, we carried out the same investigation for the eclipse period. A spin satellite such as GMS-5 has an eclipse period of approximately 50 days in spring (from the end of February to the middle of April) and in autumn (from the end of August to the middle of October). Therefore, variability of effective shutter temperature (Te) becomes large in V16 (observation at 16UTC), observation immediately after the eclipse period is finished. Te at V16 has large periodic variation from about 283K to about 295K as shown in Figure 7.

Coefficient d in Eq. (6), which represents the relation between the digital count and radiance, has large periodic variation as shown in Figure 8, due to the variability of Te. We had statistics of temperature difference between the previous table and the day table using the data of V16 (340 in number) during the eclipse period from August 30, 1995 to March 6, 1999. The result shows that the mean of error, standard deviation and maximum error are 0.00K, 0.23K and 0.81K respectively, for the 150 level of IR1 and 0.00K, 0.24K and 1.02K for the high temperature region of IR2. Thus, standard deviation and maximum error for V16 (eclipse period) are about 1.5 times and 1.8 times larger than that for V0, respectively. The mean of error and standard deviation are 0.00K and 0.15K respectively for the lower temperature region of IR1, IR2 and WV, however, the maximum error is largest for IR2 (0.65K), followed by IR1 (0.52K) and WV (0.40K). Thus, standard deviation and maximum error for V16 (eclipse period) are about 1.5 times and about 1.3 ~ 1.7 times larger than that for V0, respectively for the lower temperature region.

Thus, we found out that error increases as temperature increases and error at V16 during the eclipse period further increases. In addition, we found out that error of IR2 is largest among the three infrared channels. Therefore, it is necessary for us to take account of these errors when we analyze a series of infrared brightness temperature data and evaluate the physical values estimated from infrared data.

3.3 Calibration in Wind Observations

We carried out observations (hereafter referred to as wind observation) for estimating atmospheric motion wind (AMW) at 30 minutes before normal observation four times a day (00, 06, 12, 18UTC) using GMS-5. We used the same calibration table for wind observation as that used for normal observation 30 minutes later due to the limited capacity of the computer in CDAS.

We investigated the relation between the difference in observation time and the difference in the

Table 3 Temperature difference between the table for the day and for the previous day.
The upper side is normal, while the lower side is in eclipse.

Channel	Level	Temp. (K)	Vias (K)	RMS (K)	Max Diff. (K)	Level	Temp. (K)	Vias (K)	RMS (K)	Max Diff. (K)
IR1(V0)	150	290	0.00	0.15	0.48	60	235	0.00	0.10	0.39
IR2(V0)	150	290	0.00	0.16	0.56	60	235	0.00	0.10	0.39
WV(V0)	-	-	-	-	-	40	245	0.00	0.10	0.31
IR1(V16 Eclips)	150	290	0.00	0.23	0.81	60	235	0.00	0.15	0.52
IR2(V16 Eclips)	150	290	0.00	0.24	1.02	60	235	0.00	0.15	0.65
WV(V16 Eclips)	-	-	-	-	-	40	245	0.00	0.14	0.40

Table 4 Temperature difference between the table produced using observation data and the table before one hour. (temperature difference between V0 and V1 at the same level)

Channel	Level	Temp. (K)	Vias (K)	RMS (K)	Max Diff. (K)	Level	Temp. (K)	Vias (K)	RMS (K)	Max Diff. (K)
IR1	150	290	0.00	0.13	0.46	60	235	0.00	0.11	0.52
IR2	150	290	0.00	0.14	0.60	60	235	0.00	0.10	0.46
WV	-	-	-	-	-	40	245	0.00	0.11	0.39

calibration table to make clear the effect of using the calibration table in the normal observation for wind observation instead of the real calibration table.

Table-4 shows the statistics of temperature difference (error) between the calibration table produced by data observed one hour before and that at the time of the level of the high and low temperature regions. The mean of error, standard deviation and maximum error are 0.00K, 0.13K and 0.81K respectively for the 150 level corresponding to the high temperature region of IR1. Also the mean of error, standard deviation and maximum error are 0.00K, 0.14K and 0.60K respectively for the 150 level corresponding to the high temperature region of IR2. The mean of error and standard deviation are 0.00K and 0.10K respectively. However, the maximum error is largest (0.52K) for IR1, followed by IR2 (0.46K) and WV (0.39K).

We should consider the error due to the temperature difference which occurred by using the calibration table 30 minutes later and using the previous table. The greatest effect occurred when we estimated the altitude of the AMW from the cloud top temperature. The error estimated and altitude of AMW is approximately 20 m, at least assuming the decreasing rate of air temperature is 0.6 K / 100 m since maximum error of cloud top temperature is approximately 1K.

3.4 Error for S-VISSR Fixed Table

The calibration table for S-VISSR is produced as the temperature difference between the S-VISSR table and the fixed table at 200K reach minimum. It causes a tendency for a large temperature difference between the real calibration table and the fixed table.

Figure 9 shows the temperature difference between the IR1 calibration table of S-VISSR and the fixed IR1 calibration table for the level corresponding to every 20K from 240K to 300K of the IR1 calibration table of S-VISSR. It shows a tendency for the temperature difference to become larger as temperature increases. The fixed table was modified in March 1, 1996 to reflect the characteristic of temperature on orbit. It causes a temperature difference of at least 4 K and the temperature of the fixed table is larger than that of S-VISSR before modification, while the temperature difference is at least -2.5 K and the temperature of the fixed table is

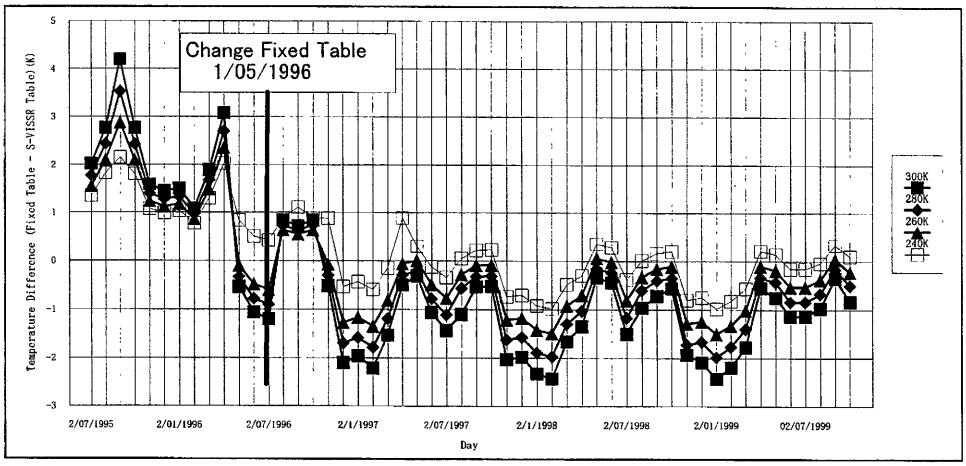

Figure 9 The temperature difference between IR1 calibration table of S-VISSR and the fixed IR1 table for the level corresponding to every 20K from 240K to 300K of IR1 calibration table of S-VISSR.

lower than that of S-VISSR. In addition to that, it indicates the seasonal variation as the temperature of the fixed table becomes lower still in January and in July.

In addition, we investigated for IR2 and WV. The result shows that the temperature difference for 300K of IR2 is at least -2.4K and that for 250K of WV is at least -2.5K. It is necessary to take note of this for utilization of the fixed table.

3.5 Response Function

Dr. Breon at NOAA pointed out that the response function of water vapor on board GMS-5 is very similar to the curve of transitivity of water vapor in the atmosphere (Breon, 1999, private communication). Response function shows the rate of energy at specific wavelengths caught by the detector in vacant. The response function was produced by observing energy emitted from a target 4 ～ 6 m apart from the detector on the ground before launch by the satellite production company. The experiment should be carried out in vacant to delete the effect of absorption and reflection by gases in the atmosphere. Thus, it appears that not all of the energy emitted from a target reaches the detector since the experiment is carried out in the atmosphere. As a result, the response function is affected by water

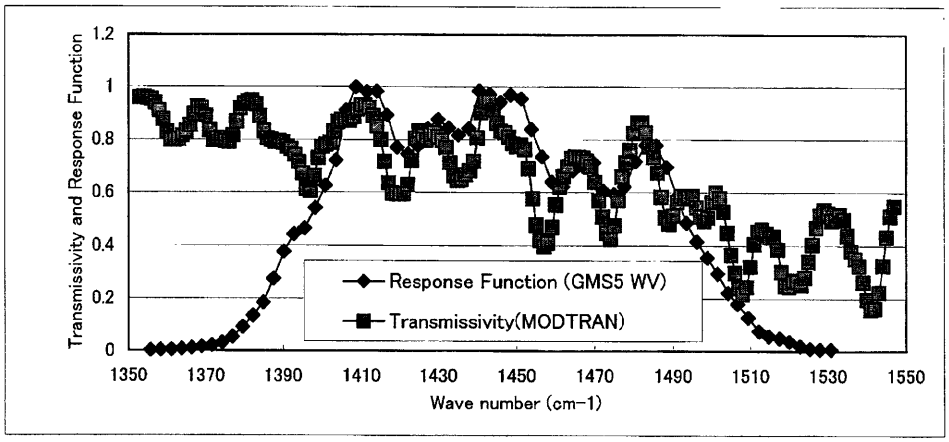

Figure 10 The curve of transmissivity in the atmosphere at the 4 m path horizontally in surface (1013hPa) calculated by using the radiative transfer model (MODTRAN) and the 1976 USA Standard Atmospheric Model overlying the response function of the water vapor channel.

vapor et al.. The effect of water vapor is very small for IR1 and IR2 channels since the wavelength of observation of IR1 and IR2 is a window region in the atmosphere, while it is very large for the WV channel since the wavelength of observation of WV is the water vapor absorption region.

In the Meteorological Satellite Center, JMA, we compared the response function of water vapor with transmissivity in the atmosphere at a 4 m path horizontal surface (1013hPa) using radiative transfer model (MODTRAN, Berk, 1989, Kneizys, 1988) and 1976 USA Standard Atmospheric Model (Kneizys, 1988). Figure 10 shows the curve of estimated transmissivity overlying the response function of the water vapor channel. We assumed the similarity as indicated by Dr. Breon.

At present, we are considering the effect of calibration by response function and a method to correct the effect in MSC.

4. Notes on Utilization of Visible Channel Data

It was reported that the sensitivity of visible detectors (PMT) has a long term change by analyzing visible data for a long time from GMS-3 and GMS-4 (Tsuchiya 1996). Fortunately, the visible detector of GMS-5 becomes a Silicon-Photo-Diode with a stable condition instead of PMT. It is important for us to get a long term variety for visible data to use visible data for a long time.

We compared the long term change of the visible channel data of GMS-5 with that of GMS-4. We used the histogram produced from the digital count of GMS full image data at V6 in GMS-4 (from December 9, 1989 to May 15, 1995) and GMS-5 (from June 13, 1995 to March 31, 1999). We first got the counts corresponding to 40 %, 70%, 90%, 98%, 99.9% from the zero count side in the accumulated histogram. Then the counts are converted, the reflectance and a series of reflectance are evaluated.

Figures 11 and 12 show the change of the above reflectance of GMS-4 and GMS-5 respectively. In GMS-4, 2.75 % of the reflectance when operation of GMS-5 started decreases to 1.67 % of the reflectance five and half years later in the 40 % of accumulated frequency corresponding to the lower reflectance level. In addition, 68.72 % of the reflectance when the operation of GMS-5 started decreases to 51.89% of the reflectance five and half years later in the 99.9 % of accumulated frequency corresponding to the higher reflectance level.

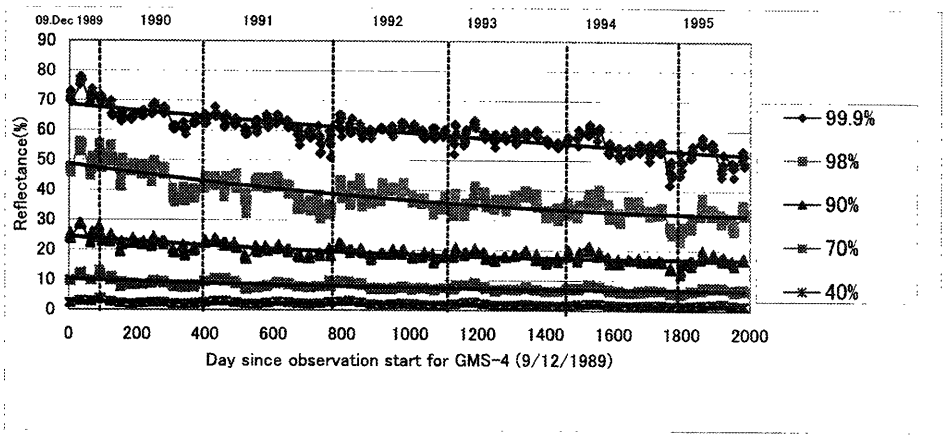

Figure 11 The annual change of visible reflectance of GMS-4
The reflectance corresponding to 40%, 70%, 90%, 98%, 99.9% from the lower side on the accumulated histogram produced from GMS full image data at V6 in GMS-4 (from 9 December 1989 to May 15 1995).

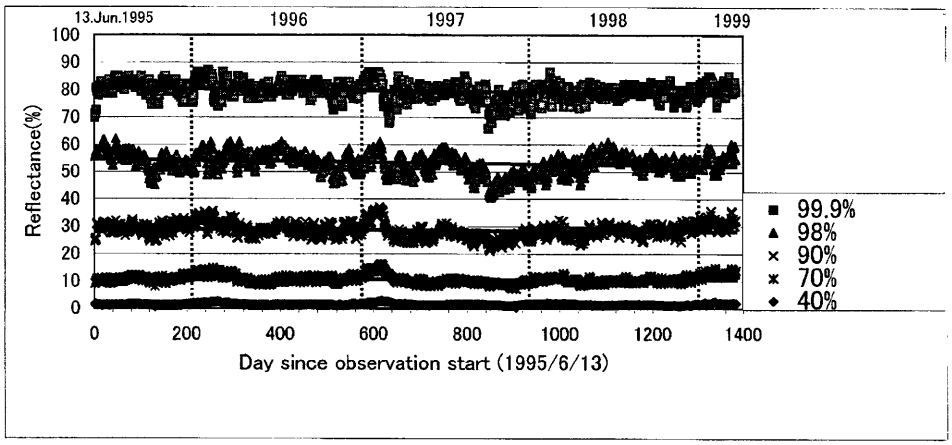

Figure 12 The same as Figure 11 except for GMS-5 (from June 13 1995 to 31 March 31 1999).

On the other hand, in GMS-5, 1.56 % of the reflectance is not changed at the time between when operation of GMS-5 started and four years later. Thus, there is no decrease in level. Also, 80.87 % of the reflectance when operation of GMS-5 started decreases to 78.38 % of the reflectance four years later in the 99.9 % of accumulated frequency. Thus, the rate of decreasing is about one level.

Thus, it is considered that the decreasing rate of the visible channel of GMS-5 is smaller than that of GMS-4.

5. Calibration Method for Emergency Cases When Calibration Shutter Data Are Not Available

With the in-flight calibration methods of the infrared channels, the VISSR uses a blackbody and a calibration shutter. The blackbody temperature as a reference is measured during the performance of the hourly VISSR observation using the calibration shutter.

By synchronizing with the satellite rotation, the shutter controls whether to convert the incoming radiation energy from the blackbody to the detectors or the incoming energy from the mirrors to the detectors.

Soon after the in-orbit test period of GMS-5 began, however, a phenomena occurred where the incoming radiation energy from the blackbody had often got into the field of view of the sensors while the sensors were scanning the earth. It happened because the motion of the shutter did not synchronize with the satellite rotation. This is called the unlocked shutter condition.

To avoid interference with the signals on images, we changed the operation of the shutter as follows: Namely, we turned off the shutter's electric current immediately after getting the calibration data, and then we turn it on when the sensors finished scanning the earth. We started operation of the shutter on August 9, 1995. With this operation, we have been able to obtain normal images up to now.

However, the following issues correspond to the utilization of GMS-5 over its lifetime:

- The possibility of changing the unlocked shutter condition from the normal condition.
- The possibility of problems with the shutter due to the payload of the on-off operation.

Therefore, it is necessary to develop an alternative method, which does not require calibration shutter information. The essence of the method is the use of housekeeping telemetry data on the temperature of various parts of VISSR.

5.1 The Non-eclipse Period

A principle of the operational calibration method of IR channels of GMS-5 VISSR depends upon the linear relation between incoming IR radiance and the output voltage of the IR channel. Taking space as a cold source and a calibration shutter in VISSR as a high source, a calibration regression equation to convert the output voltage of the IR channel into temperature is determined.

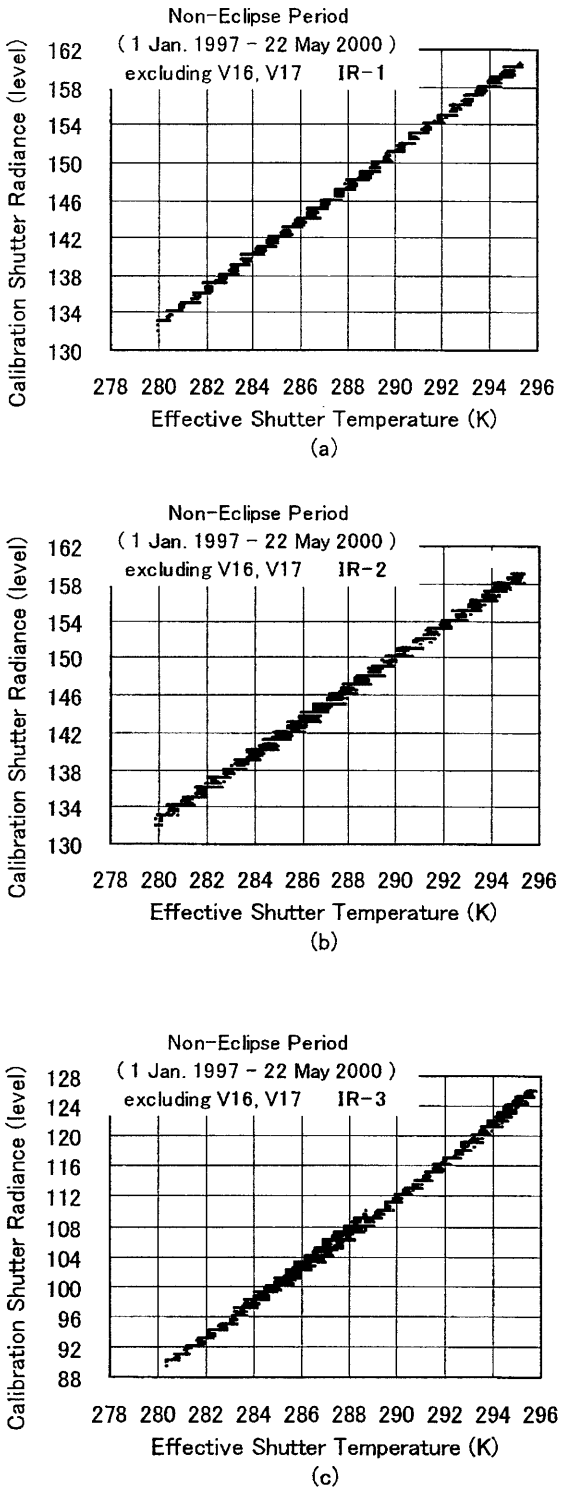

Figure 13 Relation between the Effective Shutter Temperature and the Calibration Shutter Radiance during the normal period (1 Jan. 1997 - 22 May 2000) excluding V16 and V17 during the eclipse period. (a): IR-1, (b): IR-2, (c): IR-3.

In this report we statistically estimated a digital count (Sh) (calibration shutter radiance) corresponding to the output voltage when VISSR views the calibration shutter, assuming that a linear relation exists between the output voltage when VISSR views the calibration shutter under normal conditions and the effective shutter temperature (Te) estimated from housekeeping telemetry data.

Utilizing the hourly data under normal conditions during the period from January 1, 1997 through May 22, 2000 excluding V16 and V17 during the eclipse period, analysis was made of the relationship between the calibration shutter radiance and the effective shutter temperature. The results of IR-1, IR-2 and IR-3 are shown in Figures 13 (a), (b) and (c) respectively. The ordinate is the effective shutter temperature and abscissa is the digital count of the calibration shutter radiance. It can be seen that there is a good linearity in the relationship of the two items. Based on this analysis, Eq. (11) is derived.

$$Sh = a\,Te + b \qquad (11)$$

where Sh and Te are the calibration shutter radiance level and effective shutter temperature (K) respectively, while a and b are constants.

In Table 5 the values a, b, correlation coefficient (R) and the standard error of estimation for dependent data are shown. The standard error is less than one level.

Furthermore, the above data is allocated between

Table 5 The Values of a and b of Eq. (11), Correlation Coefficient (R) and Standard Error (in Digital Count) of Estimation of Calibration Shutter Radiation from Effective Shutter Temperature for Dependent Data

Channel	Coefficients		Correlation Coefficient (R)	Standard Error
	a	b		
IR-1	1.826	-378.56	0.999	0.28
IR-2	1.720	-348.96	0.997	0.36
IR-3	2.407	-585.91	0.998	0.48

Table 6 The Values of a and b of Eq. (11), Correlation Coefficient (R) and Standard Error (in Digital Count) of Estimation of Calibration Shutter Radiation from Effective Shutter Temperature for Dependent Data (StdErrD) and Independent Data (StdErrI) in Case (1), Difference is Standard Error Difference between Independent data and Dependent data.

Channel	Coefficients		Dependent		Independent	Difference
	a	b	R	StdErrD	StdErrI	Δ StdErr
IR-1	1.8263	-378.7463	0.9986	0.2821	0.2965	0.0144
IR-2	1.7229	-349.6655	0.9979	0.3256	0.4607	0.1351
IR-3	2.3993	-583.6852	0.9977	0.4897	0.5010	0.0113

dependent data and independent data as in the following three cases, and then the above method is evaluated for independent data:

(1) Dependence data: from January 1, 1997 to December 31, 1998. Independence data: from January 1, 1999 to December 31, 1999.

(2) Dependence data: from January 1, 1998 to December 31, 1999. Independence data: from January 1, 1997 to December 31, 1997.

(3) Dependence data: from January 1, 1997 to December 31, 1999 except from January 1, 1998 to December 31, 1998. Independence data: from January 1, 1998 to December 31, 1998.

The results show that the method is effective since the standard error of estimation difference between dependence data and independence data is very small, and with the F-value at 0.05 %, confidence for independence data exceeds the standard value in all cases. For example, the statistic in case (1) is shown in Table 6.

5.2 The Eclipse Period

A similar analysis is made for the data of the eclipse period, which indicates that there is a deviation from the linear condition. Examples of vernal eclipse and autumnal eclipse are shown in Figures 14 and 15 respectively. Compared with the previous case, a little deviation from linearity is noticed. Especially the characteristic is districted in IR-1 and IR-2 for V16 in a vernal eclipse since there is about a 5-count difference at an effective shutter temperature of 290 K compared with the non-eclipse period. It is considered that the cause of this difference is due to over cooling of the detector during the eclipse period. Further analysis indicates that there is a correlation between the detector temperature control voltage and deviation in shutter radiance from normal conditions.

Analysis is made by adding the detector temperature control voltage V to Eq. (11) as shown in Eq. (12).

$$Sh = a\,Te + bV + c \qquad (12)$$

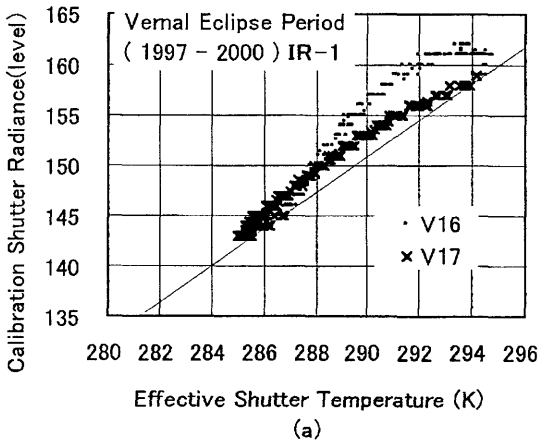

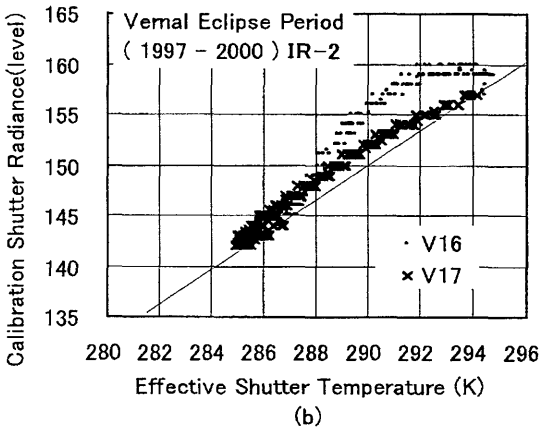

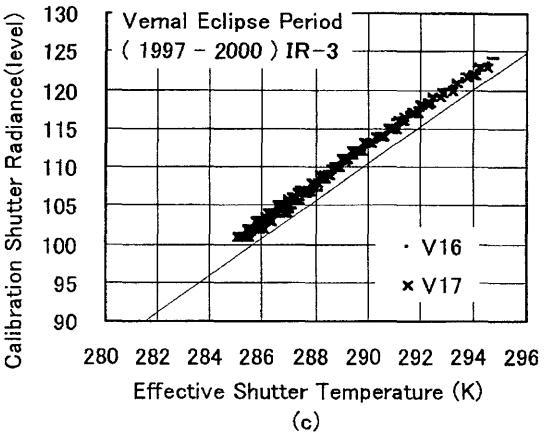

Figure 14 The same as Fig. 13 except for during the vernal eclipse.

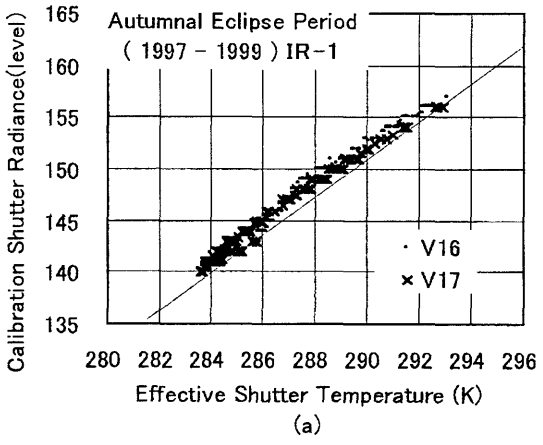

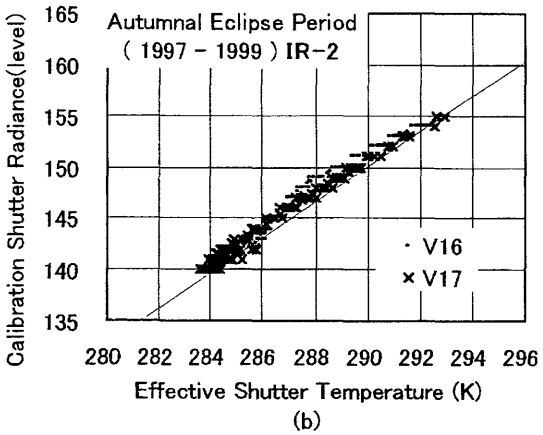

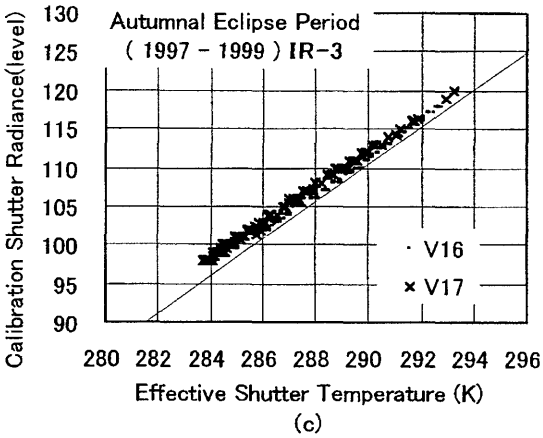

Figure 15 The same as Fig. 13 except for during the autumnal eclipse.

where a, b and c are constants.

The obtained values of a, b and c, standard error and coefficient of determination are shown in Table 7 together with that obtained from Te only. It can be seen that the result is improved compared with Te only especially in window channels. The error is almost the same as that of utilizing the calibration shutter information.

Furthermore, the above data is allocated between

Table 7　The Coefficients of Eq. (2) and Accuracy to Estimate Shutter Radiance from Effective Temperature and Detector Temperature Control Voltage. A.E.: Autumnal Eclipse, V.E.: Vernal Eclipse, S.Err: Standard Error, R: Coefficient of Determination. The Standard Error and Coefficient of Determination for the Case of Te only is shown for Comparison.

CH.	Eclipse	Coefficients					Case of Te Only	
		a	b	c	S.Err	R	S.Err	R
IR-1	A.E.	1.778	0.668	-365.67	0.535	0.994	0.634	0.983
	V.E.	1.891	2.173	-401.62	0.893	0.989	1.552	0.936
IR-2	A.E.	1.664	0.825	-334.03	0.526	0.993	0.674	0.978
	V.E.	1.772	2.320	-368.80	0.943	0.987	1.651	0.921
IR-3	A.E.	2.300	-1.011	-552.30	0.365	0.998	0.641	0.988
	V.E.	2.473	-0.238	-603.98	0.537	0.997	0.555	0.994

Table 8　The Coefficients of Eq. (2) and Accuracy Shutter Radiance from Effective Temperature and Detector Temperature Control Voltage. A.E.: Autumnal Eclipse, V.E.: Vernal Eclipse, S.Err: Standard Error, R: Coefficient of Determination. The Standard Error and Coefficient of Determination for the Case of Te only is shown for Comparison.

CH.	Eclipse	Coefficients			Dependence		Indepen.	Diff.
		a	b	c	R	StdErrD	StdErrI	△ StdErr
IR-1	A.E.	1.7809	0.6365	-366.2676	.9882	.5358	.5422	.0121
	V.E.	1.8908	2.2098	-401.5630	.9779	.9194	.8825	.0491
IR-2	A.E.	1.6574	0.8208	-332.1490	.9878	.5115	.5857	.0631
	V.E.	1.7652	2.3753	-366.7207	.9740	.9543	.9880	.0930
IR-3	A.E.	2.2971	-1.0403	-551.4956	.9965	.3604	.3841	-.0289
	V.E.	2.4624	-0.2150	-600.9214	.9936	.5583	.5296	.0321

dependent data and independent data in the same way as in the previous session, and then the above method is evaluated for independent data.

The results show that the method is effective since the standard error of estimation difference between the dependence data and the independence data is very small, and with the F-value at 0.05 %, confidence for independence data exceeds the standard value in all cases. For example, the statistic in the same period as case (1) of the previous session is shown in Table 8.

6. Summary

We report on the status of calibration of VISSR of GMS-5 and matters requiring care when users use the VISSR data in this report. We also report on the development of a new method without calibration shutter information against mal-functioning of the calibration shutter system. The content is summarized as follows:

(1) The visible channel consists of four detectors and a fixed calibration table is prepared for every detector. In S-VISSR four calibration tables are modified to the standard calibration table.

(2) The calibration procedure of the infrared channel is carried out every normal observation (24 times in a day) in DPC and the calibration table is produced. In this calibration table, the lower and higher temperature regions are corresponded to the lower and higher brightness levels respectively. In S-VISSR calibration table is produced after reversed procedure

and shift procedure. In this table, the lower and higher temperature regions are respectively corresponded to the higher and lower brightness levels.

(3) We modified emissivity of standard black body to use calibration procedure of infrared channels and reproduced calibration tables from V6 June 13, 1996 to V23 November 29, 1996. In addition, we prepared the easy-conversion table for correcting temperature of infrared data accumulated past by users easily.

(4) In the infrared calibration procedure, we use calibration table produced at the previous same time. The error for the cause increases as the lower temperature region moves to the high temperature region and further increases near to the time of eclipse. Also, the error for IR2 is largest among infrared channels with approximately 1 K for maximum error. Therefore, it is necessary for us to note the error when we analyze data of infrared brightness temperature precisely and evaluate the physical value estimated from the infrared data.

(5) In wind observations, we use the same calibration table used in normal observation 30 minutes later. This error and the use of the previous calibration table affect the estimation altitude of AMW from cloud top temperature. As the maximum error is approximately 1K, the estimated error for an altitude of AMW is 200 m at maximum, assuming 0.6 K / 100 m at a raps rate of temperature.

(6) The fixed calibration table for S-VISSR was modified in May 1, 1996. The fixed calibration table is approximately 4 K at maximum, higher than S-VISSR table at IR1 (300K) before modification, while inverse the fixed calibration table is approximately 2.5 K, at maximum lower than the S-VISSR table at IR1 (300K) after modification. There is seasonal variability in which the temperature of the fixed calibration table becomes lower in January and in July. The calibration table for IR2 and WV has the same tendency as the fixed calibration table for S-VISSR is approximately 2.4 K for IR2 (300K) and 2.5 K for WV (250K) lower than the S-VISSR calibration table.

(7) The response function of the water vapor channel of GMS-5 is similar to transmisivity of water vapor. It is assumed to be the main cause that the experiment wasn't carried out in vacant.

(8) The visible detector of GMS-5 is changed from PMT to a Silicon-Photo-Diode with more stable sensitivity. Therefore, a long-term degradation which was remarkably found in GMS-4 becomes small in GMS-5 and the rate of degradation is approximately one level four years after the operation of GMS-5 was started.

(9) A new method without the calibration shutter information is developed against mal-functioning of the calibration shutter system, which occurs irregularly. This method provides nearly the same accurate calibration data as the one using the calibration shutter information.

Furthermore, in the next generation MTSAT-1R the data resolution of the infrared channel will be changed from 8 bits to 10 bits. To cope with high temperature resolution we are expected to perform more accurate calibration. Also it is necessary to have more accurate calibration data globally for more accurate satellite data globally for investigating climate change et al.. CGMS in 1997 proposed the intercalibration between the gestational meteorological satellite and the polar orbit satellite NOAA to produce the global calibration data uniformly and to increase the quality of calibration data. Satellite operational countries including Japan carried out the investigation following the proposal.

The meteorological satellite center continues its efforts to provide more accurate calibration data.

ACKNOWLEDGEMENTS

We thank Dr. Francois-Marie Breon in NOAA / ERL for important comments to response function of water vapor channel.

REFERENCES

Berk, A., L.S. Bernstein and D.C. Roberson, 1989: MODTRAN: A Moderate Resolution Model for LOWTRAN 7, GL-TR-89-0122.

Kneizys, F.X., E.P. Shettle, L.W. Abreu, J.H. Chetwynd, G.P. Anderson, W.O. Galley, J.E.A. Selby and S.A. Clough, 1988: Users Guide to LOWTRAN 7, AFGL-TR-88-0177.

Kurihara, S. and M. Tokuno, 2000: The status of calibration of VISSR on board GMS-5, Meteorological Satellite Center Technical Note, 38, 53-68*.

McMillin, M.L. and D.S. Crosby, 1984: Theory and Validation of the Multiple Window Sea Surface Temperature Technique, J. Geophys. Res., 89, 3655-3661.

Meteorological Satellite Center, 1996: Meteorological Satellite Center Technical Note Special Issue (1996), 1-179.

Meteorological Satellite Center, 1997: The GMS User's Guide Third Edition.

Potts, R.J., 1993: Satellite Observations of Mt. Pinatubo Ash clouds, Australian Met. Mag., 42, 59-68.

Tokuno, M., 1997: Satellite observation of volcanic ash clouds, Meteorological Satellite Center Technical Note, 33, 29-48.

Tokuno, M., H. Itaya, K. Tsuchiya and S. Kurihara, 1997: Calibration of VISSR On-board GMS-5, Adv. Space Res., 19, 9, 1297-1306.

Tsuchiya, K., R. Ito and C. Ishida, 1982: Characteristics of the Detector of Multi Spectral Scanner (MSS) of Landsat in a Space Environment. J. Meteorological Soc. Japan, SerII, 60, 1165-1174.

Tsuchiya, K., M. Tokuno, H. Itaya and H. Sasaki, 1996: Calibration of GMS-VISSR, Features of MOS-VTIR and LANDSAT MSS, Adv. Space Res., 17, 1, 1-10.

*Original text in Japanese.

オペレーショナルなGMS-5 VISSRキャリブレーション

徳野　正己*、栗原　茂久*、海藤　幸広*

本報告では、外国のGMSデータの利用者のために「GMS-5 VISSRキャリブレーションの現状」（栗原、徳野、2000）の邦文を英文に修正した内容に加えて、GMS-5の運用の延長に伴い、しばしば生じていたキャリブレーションの黒体シャッターの不具合に対応するために、黒体シャッターを使用しないキャリブレーションの方法の開発について報告されている。

ここでは、はじめに以下のようなGMS-5のキャリブレーション処理状況と利用上の留意点について報告されている。

—可視及び赤外チャンネルキャリブレーションの方法

—過去データの赤外チャンネルキャリブレーションテーブルの修正

—赤外チャンネルキャリブレーションテーブル（風観測時も含む）およびVISSR固定キャリブレーションテーブルの運用上の問題点

—水蒸気チャンネルの応答関数に対する疑問点

—可視チャンネルデータの経年変化

最後に、黒体シャッターを使用しないキャリブレーションの方法が完成し、その方法での精度は黒体シャッターを使用した場合と同程度であることが示されている。